

The water/ceria(111) interface: Computational overview and new structures

Cite as: J. Chem. Phys. **152**, 104709 (2020); <https://doi.org/10.1063/1.5142724>

Submitted: 18 December 2019 . Accepted: 05 February 2020 . Published Online: 10 March 2020

Andreas Röckert , Jolla Kullgren , Peter Broqvist , Seif Alwan, and Kersti Hermansson 

COLLECTIONS

Paper published as part of the special topic on [Oxide Chemistry and Catalysis](#)

Note: This paper is part of the JCP Special Topic on Oxide Chemistry and Catalysis.



View Online



Export Citation



CrossMark

ARTICLES YOU MAY BE INTERESTED IN

[Vibrational properties of CO₂ adsorbed on the Fe₃O₄ \(111\) surface: Insights gained from DFT](#)

The Journal of Chemical Physics **152**, 104702 (2020); <https://doi.org/10.1063/1.5136323>

[Molecular polaritons for controlling chemistry with quantum optics](#)

The Journal of Chemical Physics **152**, 100902 (2020); <https://doi.org/10.1063/1.5136320>

[Anharmonic calculations of vibrational spectra for molecular adsorbates: A divide-and-conquer semiclassical molecular dynamics approach](#)

The Journal of Chemical Physics **152**, 104104 (2020); <https://doi.org/10.1063/1.5142682>

Lock-in Amplifiers

Find out more today



Zurich
Instruments



The water/ceria(111) interface: Computational overview and new structures

Cite as: J. Chem. Phys. 152, 104709 (2020); doi: 10.1063/1.5142724

Submitted: 18 December 2019 • Accepted: 5 February 2020 •

Published Online: 10 March 2020



View Online



Export Citation



CrossMark

Andreas Röckert,  Jolla Kullgren,  Peter Broqvist,  Seif Alwan, and Kersti Hermansson^{a)} 

AFFILIATIONS

Department of Chemistry – Ångström Laboratory, Uppsala University, Box-538, Uppsala SE-75121, Sweden

Note: This paper is part of the JCP Special Topic on Oxide Chemistry and Catalysis.

^{a)} Author to whom correspondence should be addressed: kersti@kemi.uu.se. URL: <http://www.teoroo.kemi.uu.se/>

ABSTRACT

Thin film structures of water on the CeO₂(111) surface for coverages between 0.5 and 2.0 water monolayers have been optimized and analyzed using density functional theory (optPBE-vdW functional). We present a new 1.0 ML structure that is both the lowest in energy published and features a hydrogen-bond network extending the surface in one-dimension, contrary to what has been found in the literature, and contrary to what has been expected due to the large bulk ceria cell dimension. The adsorption energies for the monolayer and multilayered water structures agree well with experimental temperature programmed desorption results from the literature, and we discuss the stability window of CeO₂(111) surfaces covered with 0.5–2.0 ML of water.

© 2020 Author(s). All article content, except where otherwise noted, is licensed under a Creative Commons Attribution (CC BY) license (<http://creativecommons.org/licenses/by/4.0/>). <https://doi.org/10.1063/1.5142724>

I. INTRODUCTION

The interaction of water with solid oxide surfaces is of critical importance in many environmentally and technologically relevant processes, including electrochemistry, corrosion, catalysis, atmospheric chemistry, and photocatalytic water splitting (see, for example, Refs. 1 and 2). One such oxide is CeO₂ (ceria) relevant in all the aforementioned applications as well as in a range of emerging ones such as solid oxide electrolysis cells,³ hydrophobic coatings,⁴ and bio-medicine.⁵ Scientifically, the mechanisms underpinning these applications are all very complex and particularly so by virtue of the structure and properties of the oxide material itself, its surface terminations, its acid–base properties, and the possible presence of defects, all of which influence adsorption of water. Molecular-level insight concerning where and how the water molecules bind to the ceria surface is a prerequisite to building mechanistic models that can handle such scenarios. In this paper, we aim to review previous findings and elaborate on the interface structures at low water coverages on ceria(111), in search of extended hydrogen-bond patterns using density functional theory (DFT).

In the last two decades, considerable efforts have been made to explore thin water films (up to a few monolayers) on ceria using a range of experimental methods such as X-ray photoelectron

spectroscopy (XPS),^{6–9} temperature programmed desorption (TPD),^{6–10} and scanning force microscopy (SFM).^{11,12} The experimental evidence suggests that water molecules in thin water films on ceria(111) partially dissociate, i.e., there is coexistence of H₂O and OH.^{7–9,11} Moreover, it is quite well established that water molecules (intact or dissociated) adsorb above exposed cerium cations as shown in Ref. 11, but the details of the interface structure have not been possible to decipher by experimental methods. Here, computational studies can provide valuable information.

Indeed, a significant number of computational studies have been published for water on ceria(111) with the aim to elucidate the interface structure and quantify the water–water and water–surface interactions.^{4,13–25} All periodic quantum-mechanical (QM) studies that we are aware of for water/ceria(111) are listed in Table I, except for Ref. 23, which is an *ab initio* MD simulation of a water film on stoichiometric ceria(111) at room temperature. It should be noted that Refs. 19 and 21 contained a large number of monomer calculations; all their smaller cell results were not included in our table. In summary, the rightmost column in Table I shows that, to date, all stable structures found by total energy minimization at coverages up to and including 1.0 ML coverage (monolayer is defined in Sec. II) consist of individual water molecules or finite clusters of water molecules, adsorbed on the surface. For higher water

TABLE I. Theoretical work on adsorption of water on the ceria (CeO_2) (111) surface, ordered by surface coverage. *First column:* Reference. *Second column:* Water coverage (see definition in text). *Third column:* Q is the fraction of dissociated water molecules out of the total number of adsorbed molecules. *Fourth column:* Surface supercell size used. *Fifth column:* Reported adsorption energies. For some entries, two energy values are given; the first refers to the most stable structure obtained and the second to the second most stable structure (when reported with the same coverage, cell, Q, and method). For some other entries, additional values in brackets, [], are given, namely, in the cases where we have started from the reported structure and reoptimized using optPBE-vdW with our computational protocol; in all those cases, we reproduced the published structure as far as we could judge. *Sixth column:* Program and method. *Seventh column:* A short description of our interpretation of the hydrogen-bond motif described in each reference. *General:* The last three entries are three new structures found in this work.

References	Coverage	Surface cell	Q	E_{ads} (eV/ H_2O)	Method	Structural motif
Kropp ²¹	0.0625	4 × 4	0	−0.53	VASP, PBE+U (4.5 eV)	Intact monomer
Kropp ²¹	0.0625	4 × 4	0	−0.66	VASP, PBE+U (4.5 eV) +D2	Intact monomer
Kropp ²¹	0.0625	4 × 4	1	−0.59	VASP, PBE+U (4.5 eV)	Dissociated monomer
Kropp ²¹	0.0625	4 × 4	1	−0.73	VASP, PBE+U (4.5 eV) +D2	Dissociated monomer
Kropp ²¹	0.0625	4 × 4	0	−0.54	VASP, HSE	Intact monomer
Kropp ²¹	0.0625	4 × 4	0	−0.66	VASP, HSE+D2	Intact monomer
Kropp ²¹	0.0625	4 × 4	1	−0.63	VASP, HSE	Dissociated monomer
Kropp ²¹	0.0625	4 × 4	1	−0.73	VASP, HSE+D2	Dissociated monomer
Fernández-Torre ¹⁹	0.1111	3 × 3	0	−0.55	VASP, PBE+U (4.5 eV)	Intact monomer
Fernández-Torre ¹⁹	0.1111	3 × 3	1	−0.60, −0.17	VASP, PBE+U (4.5 eV)	Dissociated monomer
Fernández-Torre ¹⁹	0.1111	3 × 3	0	−0.67	VASP, optPBE-vdW+U (4.5 eV)	Intact monomer
Fernández-Torre ¹⁹	0.1111	3 × 3	1	−0.67, −0.23	VASP, optPBE-vdW+U (4.5 eV)	Dissociated monomer
Fernández-Torre ¹⁹	0.1111	3 × 3	0	−0.73	VASP, optB86b-vdW+U (4.5 eV)	Intact monomer
Fernández-Torre ¹⁹	0.1111	3 × 3	1	−0.76, −0.32	VASP, optB86b-vdW+U (4.5 eV)	Dissociated monomer
Kropp ²¹	0.125	4 × 4	0.5	−0.68	VASP, PBE+U (4.5 eV)	Dimer
Molinari ¹⁸	0.167	2 × 3	0	−0.58	VASP, PBE+U (5 eV)	Intact monomer
Molinari ¹⁸	0.167	2 × 3	1	−0.59	VASP, PBE+U (5 eV)	Dissociated monomer
Watkins ¹⁵	0.25	2 × $\sqrt{2}$	0	−0.32	VASP, PW91	Intact monomer
Watkins ¹⁵	0.25	2 × $\sqrt{2}$	0	−0.36	VASP, PW91 + U (5 eV)	Intact monomer
Watkins ¹⁵	0.25	2 × $\sqrt{2}$	1	−0.53	VASP, PW91 + U (5 eV)	Dissociated monomer
Fronzi ¹⁷	0.25	2 × 2	0	−0.49, −0.33	DMol, PBE	Intact monomer
Fronzi ¹⁷	0.25	2 × 2	1	−0.36	DMol, PBE	Dissociated monomer
Yang ²⁰	0.25	2 × 2	0	−0.57	VASP, PBE+U (5 eV)	Intact monomer
Yang ²⁰	0.25	2 × 2	1	−0.55	VASP, PBE+U (5 eV)	Dissociated monomer
Marrocchelli ²⁴	0.25	2 × $\sqrt{3}$	0	−0.51	VASP, PBE+U (5 eV)	intact monomer
Marrocchelli ²⁴	0.25	2 × $\sqrt{3}$	1	−0.37	VASP, PBE+U (5 eV)	dissociated monomer
Fernández-Torre ¹⁹	0.25	2 × 2	0	−0.49, −0.30	VASP, HSE06	Intact monomer
Fernández-Torre ¹⁹	0.25	2 × 2	1	−0.47, −0.24	VASP, HSE06	Dissociated monomer
Szabová ²⁵	0.25	2 × 2	0	−0.52, −0.51	VASP, PBE+U (4.5 eV)	intact monomer
Szabová ²⁵	0.25	2 × 2	1	−0.50, −0.24	VASP, PBE+U (4.5 eV)	dissociated monomer
Chen ¹⁴	0.3333	1 × $\sqrt{3}$	0	−0.49, −0.52	VASP, PW91	Intact monomer
Kumar ¹⁶	0.5	1 × 2	0	−0.58	VASP, GGA	No HB network
Fronzi ¹⁷	0.5	1 × 2	0	−0.50	DMol, PBE	No HB network
Molinari ¹⁸	0.5	2 × 3	0	−0.60	VASP, PBE+U (5 eV)	No HB network
Kumar ¹⁶	1.0	1 × 2	0	−0.55 [−0.713]	VASP, GGA	No HB network
Molinari ¹⁸	1.0	2 × 3	0	−0.57 [−0.713]	VASP, PBE+U (5 eV)	No HB network
Molinari ¹⁸	1.0	2 × 3	1	−0.15 [−0.360]	VASP, PBE+U (5 eV)	No HB network
Kropp ²¹	1.0	2 × 2	0.25	−0.546 [−0.679]	VASP, PBE+U (4.5 eV)	HB-tetramer
Kropp ²¹	1.75	2 × 2	0.143	−0.570 [−0.717]	VASP, PBE+U (4.5 eV)	Fully covered, HB-network
Carchini ²²	2.0	2 × 2	0	−0.20 [−0.695]	VASP, PBE+U (4.5 eV)	Hexagonal water network
Carchini ²²	2.0	2 × 2	0.125	−0.39	VASP, PBE+U (4.5 eV)	Hexagonal water network

TABLE I. (Continued.)

References	Coverage	Surface cell	Q	E_{ads} (eV/H ₂ O)	Method	Structural motif
Carchini ²²	2.0	2 × 2	0.25	−0.42	VASP, PBE+U (4.5 eV)	Hexagonal water network
Carchini ²²	2.0	2 × 2	0.375	−0.37	VASP, PBE+U (4.5 eV)	Hexagonal water network
Carchini ²²	2.0	2 × 2	0.5	−0.35	VASP, PBE+U (4.5 eV)	Hexagonal water network
Fronzi ⁴	2.0	2 × 2	0	−0.179 ^a [−0.695]	VASP, PBE+U (4.2 eV)	Hexagonal water network
Carchini ²²	4.0	2 × 2	0.125		VASP, PBE+U (4.5 eV)	Hexagonal water network
This work	0.5	1 × 4	0.5	−0.740	VASP, optPBE-vdW	1d-chain
This work	1.0	1 × 2	0.5	−0.773	VASP, optPBE-vdW	1d-chain
This work	1.5	1 × 2	0.333	−0.733	VASP, optPBE-vdW	2d-network

^a E_{ads} is not reported, only $E_{adhesion}$ is reported, which is the energy in reference to adsorption of a water film in contrast to an isolated water molecule.

coverages, starting at 1.75 ML, infinite hydrogen-bonded networks have been found, spanning the two surface dimensions, but for lower coverages, 1.0 ML or less, this is not the case.

In this paper, we continue the exploration of thin water films on ceria with special focus on the 1.0 ML case for the fully oxidized ceria(111) surface *with the aim to find if a single monolayer can form a continuous hydrogen bond network extending the surface*. The answer is *yes* and we will present a 1.0 ML structure, which not only is (slightly) more stable than all other monolayer water/ceria(111) structures presented in the literature so far but also forms a periodically repeated H-bond network in one dimension.

Another focus of this paper is the consequences—or not—of water dissociation. Considering the extremes for monolayer coverage, i.e., zero and full dissociation, the energy difference is about 0.4 eV/H₂O,¹⁸ in contrast to the tiny energy difference observed between an intact isolated water molecule on the ceria(111) surface and its dissociated counterpart (see Table I). Here, we present monolayer structures that span the full dissociation range: 0%, 25%, 50%, 75%, and 100%. Using DFT, we have optimized 13 unique monolayer structures, including the three previously reported in the literature.^{16,18,21} Although these 13 represent just a subset of all the existing energy minima on the 1.0 ML potential energy surface, they allow us to *discuss stability vs dissociation degree and structural motif* since these structures display a range of H-bond patterns. This is the second aim of this paper. For the 1.0 ML coverage, we find that partial dissociation is, in fact, more stable than the fully intact layer. Furthermore, we attempt to validate our results by simulating the TPD desorption temperatures.

This paper is organized as follows: Section II describes the electronic structure calculations, geometric structure optimization, and water adsorption starting structures. Section III A addresses our first aim and provides a condensed review of the existing literature for different coverages and a presentation of the most stable structures that we have found. Here, we also present predicted scanning tunneling microscopy (STM) images primarily as a good way to highlight differences between structural patterns. Section III B addresses the second aim, water dissociation. In Sec. III C, we relate the adsorption energies to TPD experiments from the literature, and calculations

of the stability windows for the different coverages are presented in Sec. III D.

II. METHOD

A. Surface systems

Slab structures of the non-polar, oxygen terminated ceria(111) surface were generated from the cubic fluorite structure ($Fm\bar{3}m$) of ceria with an optimized cell parameter (of bulk CeO₂) of 5.48 Å at the optPBE-vdW DFT level (see below). The experimental value is 5.41 Å (Ref. 2) at room temperature and the extrapolated 0 K cell parameter at 5.39 Å (Ref. 26). The slab systems were composed of a 12 atomic layer thick slab separated by a 30 Å wide vacuum gap, perpendicular to the surface. Four surface supercells were used corresponding to $p(1 \times 1)$, $p(1 \times 2)$, $p(1 \times 4)$, and $p(2 \times 2)$ expansions of the primitive surface unit cell.

The ceria(111) surface exposes both oxygen anions and cerium cations, where oxygen terminates the surface and cerium is found in the threefold hollow position between oxygen, recessed by 0.78 Å [see Fig. 1(a)]. Water was adsorbed on one of the two sides of the slab. The water molecules were placed in the supercells described

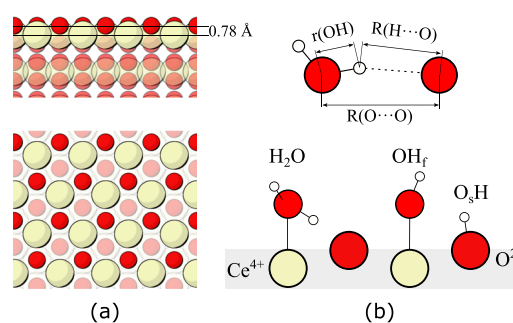


FIG. 1. Illustrations of surface systems discussed in this paper. (a) Top and side of the clean ceria(111) surface without water adsorption. (b) Definitions of hydrogen-bond distances and surface water species in this paper: intact H₂O, OH_f, and O₃H. Surface water species H₂O, OH_f, and O₃H (bottom). Atoms are colored: oxygen, red; hydrogen, white; and cerium, ivory (off white).

above at different coverages. The surface coverage is expressed in terms of monolayers (MLs), referring to the number of water molecules (intact or not) adsorbed per surface cation. In structures up to 1.0 ML coverage, water molecules were placed above the cerium cations, in the hollow site, and the coordinates were reoptimized.

Altogether 26 initial structures were examined including five structures that were taken from the literature. The five previously reported structures represent coverages of 1.0 ML from Refs. 16, 18, and 21, 1.75 ML from Ref. 21, and 2.0 ML from Ref. 4. These were built either directly from reported atomic positions or from atomic positions deduced by us by visual inspection of published figures; subsequently, they were all reoptimized by us using the optPBE-vdW method and consistent settings (as described above and in Sec. II B) concerning the number of atomic slab layers, the vacuum gap size, the cell parameters, and our computational protocol. The other 21 structures were constructed by placing water at plausible orientations in mixes of intact and dissociated water molecules according to 0%, 25%, 50%, 75%, and 100% dissociation. The degree of dissociation is henceforth abbreviated as Q-N, where N is the fraction of dissociated water molecules, i.e., Q-0.0, Q-0.25, Q-0.5, Q-0.75, and Q-1.0.

After full geometry optimization, only 17 unique structures remained. They are listed in Table II and span coverages from 0.5

to 2.0 ML. As mentioned, 13 of these pertain to the 1.0 ML coverage. In the five cases where we started with structures from the literature, our optimized structures essentially gave the same structure as the published ones. The adsorption energies for these cases are reported in brackets in the fifth column in Table I, and all our adsorption energies are listed in Table II.

A reference calculation for the gas-phase water molecule [$\text{H}_2\text{O}(\text{g})$] was simulated in a $13 \text{ \AA} \times 13 \text{ \AA} \times 13 \text{ \AA}$ box.

B. Electronic structure calculations

All calculations were performed using the Vienna *ab initio* Simulation Package (VASP version 5.4.4)^{27–30} using the optPBE-vdW functional,^{31,32} found to quite accurately describe adsorption of water on oxides³³ and in condensed systems containing H_2O and ions.³⁴ The valence states, Ce(4f, 5s, 5p, 5d, 6s), O(2s, 2p), and H(1s), were treated explicitly, and valence–core interactions were treated with the projector-augmented wave (PAW) method.^{35,36} The calculations were not spin-polarized or dipole corrected. The plane-wave basis-set was truncated at 1000 eV, and the electronic structure convergence criterion in the self-consistent-field (SCF) cycle was set to 10^{-7} eV.

The slab system's Brillouin zones were sampled using a Γ -centered $5 \times 5 \times 1$ Monkhorst-Pack grid and Blöchl tetrahedron

TABLE II. Results from our own optPBE-vdW structure optimizations. The upper part lists all 13 1.0 ML structures in order of decreasing stability. The structure label in the first column refers to the number displayed in Fig. 3. The lower part lists the stable structures that we examined for each coverage. A, 1, and B were constructed and optimized by us (and are also listed on the last three rows in Table I), while C and D were started from published structures (as is clarified in the last column).

Structure label	Coverage	Surface cell	Q ^a	E_{ads} (eV/ H_2O)	Structure from ^b
1.0 ML structures					
1	1	1×2	0.5	−0.773	This work
2	1	2×2	0.25	−0.749	This work
3	1	2×2	0.5	−0.730	This work
4	1	2×2	0	−0.716	This work
5	1	1×1	0	−0.713	Kumar ¹⁶ and Molinari ¹⁸
6	1	1×2	0.5	−0.685	This work
7	1	2×2	0.25	−0.679	Kropp ²¹
8	1	1×4	0.25	−0.661	This work
9	1	2×2	0.75	−0.603	This work
10	1	1×2	0.5	−0.602	This work
11	1	2×2	0.5	−0.599	This work
12	1	2×2	0.75	−0.557	This work
13	1	1×1	1	−0.360	Molinari ¹⁸
Coverage variation					
A	0.5	1×4	0.5	−0.740	This work
1	1	1×2	0.5	−0.773	This work
B	1.5	1×2	0.33	−0.729	This work
C	1.75	2×2	0.14	−0.717	Kropp ²¹
D	2	2×2	0	−0.695	Carchini ²² and Fronzi ⁴

^aFraction of water dissociation.

^bWhen a reference to the literature is given, the optimization was started from this structure and reoptimized by us, yielding the same overall structure. When two references are given, both refer to the same structure.

smearing of 0.1 eV was applied. For $\text{H}_2\text{O}(\text{g})$, Γ -point sampling and Gaussian smearing of 0.01 eV were utilized.

Atomic positions were optimized in the fixed supercells using the conjugate-gradient algorithm converged to forces less than 0.01 eV/Å on any and all atoms (individually and summed together). The adsorption energy was converged (to 0.005 eV) with respect to energy cutoff, k-points, and number of layers.

A Hubbard U-type correction,³⁷ which is often used in computational studies of ceria systems, was purposely not selected for this work as reduced cerium ions or oxygen vacancies were neither expected nor observed.

C. Properties

The water adsorption energy was calculated from the total energy of the optimized slab with water molecules adsorbed $E[\text{H}_2\text{O}/\text{CeO}_2]$, the optimized clean slab $E[\text{CeO}_2]$, and the optimized gas-phase molecule $E[\text{H}_2\text{O}(\text{g})]$ according to the following formula:

$$E_{\text{ads}} = -\frac{E[\text{H}_2\text{O}/\text{CeO}_2] - E[\text{CeO}_2] - nE[\text{H}_2\text{O}(\text{g})]}{n}, \quad (1)$$

where n is the number of adsorbed water molecules per supercell (intact or not), meaning that the adsorption energy is calculated per water molecule (intact or not).

In addition, we have simulated scanning tunneling microscopy (STM) images using the Tersoff–Hamann³⁸ approximation at a height of 2.0 Å above the highest located oxygen with a bias voltage of -3 eV corresponding to filled-state imaging for visualization purposes.

III. RESULTS AND DISCUSSION

A. Finite and extended water structures on ceria(111)

One of the aims of this paper, as mentioned above, is to investigate whether stable extended hydrogen-bond networks can be found for water adsorbed on the ceria(111) surface. But first, let us place this question in the context of what has been published so far.

1. Single water molecules

Adsorption of a single water molecule has been studied extensively by computational methods in Refs. 14, 15, 17, 18, 20, 21, 24, and 25 nicely summarized and somewhat definitively answered in Ref. 19. Two types of surface water species have been found, intact and dissociated water molecules [cf. Fig. 1(b)]. The dissociated water molecule is formed by transferring a H (from H_2O) to a neighboring surface oxygen, resulting in a “free” hydroxide OH_f , and a surface hydroxide O_sH (note that the negative charge is not written out in this notation). All these studies are included in Table I, labeled “monomer” and “dissociated monomer,” respectively, in the rightmost column. From these works, it has become clear that the adsorption energy difference between the intact and the dissociated water monomer is small and that adsorbed water can hydrogen bond to surface oxygen.

2. 0.5–1.0 monolayer

With the formation of a thin water film, the adsorbed species (intact or dissociated water) can not only interact with the surface

but also with other adsorbed water molecules. The 0.5 and 1.0 ML coverages were first explored by Kumar and Schelling,¹⁶ showing a marginal gain in adsorption energy per water molecule with increasing water coverage and small interactions between water molecules, but not observing any hydrogen bonds between them. Again we refer to Table I for quantitative information. A later study, by Fronzi *et al.*¹⁷ of coverages up to 0.5 ML, also observed that adsorption energies were not coverage dependent up to 0.5 ML. Molinari *et al.*¹⁸ studied 0.17–1.0 ML coverages, finding no hydrogen bonds between adsorbed water in their 1.0 ML structure, and attributed it to the largely spaced sublattice of the ceria(111) surface, an effect that had earlier been hypothesized by Henderson *et al.*⁶ In Ref. 18, each water molecule was estimated to occupy only 10 \AA^2 of the available 13 \AA^2 surface area, as calculated from the 3.88 Å distance between water adsorption sites, supporting Henderson’s hypothesis. The fully dissociated layer has also been investigated but was found to be far less stable than the fully intact layer. Kropp *et al.*²¹ proposed a new structure for the monolayer where the adsorbed water molecules form hydrogen bonds to each other in a water tetramer, with partial dissociation. Despite the increase in the total number of H-bonds in the system, the system of Kropp *et al.* was about as stable as those previously investigated. This structure included something not observed previously, namely, hydrogen bonding between adsorbed water, but not extending over to the periodically repeated image.

In this study, we found a water monolayer structure that is somewhat more stable than other published monolayer structures on ceria(111) [Fig. 2(a), $E_{\text{ads}} = 0.773 \text{ eV}/\text{H}_2\text{O}$]. It consists of an H-bond network of alternating intact and dissociated water molecules. Each OH_f ion accepts two hydrogen bonds from two water molecules ($\text{R}(\text{H}\cdots\text{O}) = 1.79 \text{ \AA}$) but does not

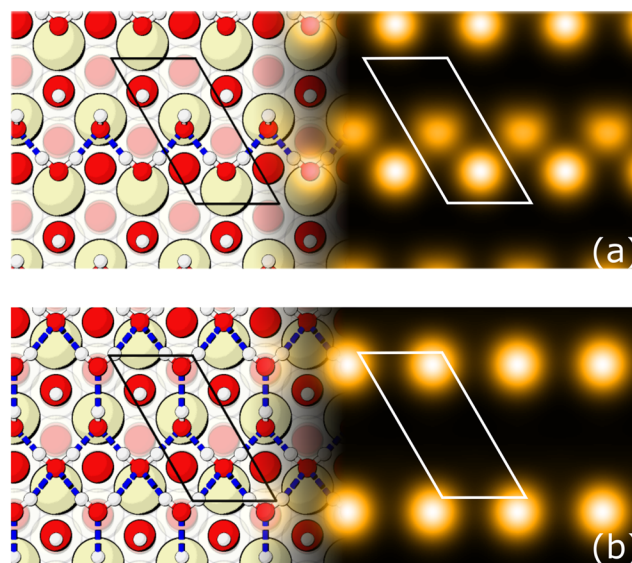


FIG. 2. Surfaces structures showing hydrogen bonds in blue (left) faded to simulated STM images using -3 eV negative bias displaying occupied states 2 Å above the water layer (right). The brightness depicts the density of states within -3 eV from the Fermi level. (a) 1.0 ML coverage, Q-0.5 (Structure 1 in Table II). (b) 1.0 ML coverage, Q-0.33 (Structure A in Table II). For atom colors, see Fig. 1.

donate any hydrogen bonds. The hydrogen bond network extends beyond the $p(1 \times 2)$ periodic boundary to produce a one-dimensional $\cdots\text{OH}_f\cdots\text{HOH}\cdots\text{OH}_f\cdots\text{HOH}\cdots$ chain with the unique building blocks being $\text{H}_2\text{O}-\text{OH}_f$ (H_3O_2^-), similar to what has been observed in calculations for the tetragonal- $\text{ZrO}_2(101)$ surface³⁹ and in a combined experimental-theoretical study for the $\text{RuO}_2(110)$ surface.⁴⁰

To ensure that this, our most stable, 1 ML structure was not constrained by the use of the (1×2) supercell, we also investigated a cell that was twice as large along the chain direction. The resulting structure was the same with respect to motifs and bond lengths.

Furthermore, we performed a computer experiment to examine the interchain interaction in this structure. The shortest oxygen-oxygen interchain distance is 5.0 Å between OH_f and H_2O in adjacent chains. Every second chain in Fig. 2(a) was removed, resulting in an oxygen-oxygen interchain distance of 11.5 Å after optimization and an E_{ads} value of 0.740 eV/ H_2O . This is 0.03 eV/ H_2O less stable than the original 1.0 ML chain structure, indicating only a weak interaction between 1D-chains at the 1.0 ML coverage. The 0.5 ML structure so obtained is listed in its own right at the bottom of Table I.

3. More than 1.0 monolayer

Thicker films have also been investigated in the literature. In their study of the hydrophobic properties of the ceria(111) surface, Carchini *et al.*²² investigated 2 and 4 ML coverages and found partial dissociation in the first layer and an infinite hexagonal H-bonded water network spanning the two surface dimensions throughout the water film. This ice-like structure was further investigated by Fronzi *et al.*⁴ for the 2.0 ML case in a study of the hydrophobicity of different ceria facets. Kropp *et al.*²¹ proposed a 1.75 ML structure consisting of an H-bonded network spanning the surface where one of the seven water molecules in the supercell was dissociated.

For coverages above 1.0 ML, we only studied a few structures and here, we also present a new stable structure for 1.5 ML coverage (C in II); the structure consists of a bottom layer, identical to the stable 1.0 ML structure, with an additional water molecule which bridges the chains ($E_{\text{ads}} = 0.729$ eV/ H_2O). This new water molecule accepts a very long $\text{OH}_f\cdots\text{OH}_2$ hydrogen-bond with $R(\text{H}\cdots\text{O}) = 2.13$ Å, and it donates two long H-bonds to the first-layer water molecules with $R(\text{H}\cdots\text{O}) = 2.09$ Å, as visualized in Fig. 2(b), thereby bridging the separate chains discussed for the monolayer. The resulting structure has a 2D-network of hydrogen bonds extending the surface.

The two stable 1.0 and 1.5 ML structures in Fig. 2 are each visualized together with a simulated STM image. These simulations serve two purposes. First, they provide an excellent way of illustrating patterns formed by the adsorbed water molecules. Second, they could provide a reference for future STM studies, although it may prove difficult to perform such experiments not least due to the low conductivity of CeO_2 . With the STM settings chosen (a negative bias of -3 V), it is the highest occupied electronic states of the adsorbed water molecules and OH_f hydroxide groups that contribute to the contrast. For the structures presented in the current investigation, the brightness in the image is closely related to the topography of the structure.

In summary, we have presented two new extended H-bonded water structures on ceria(111): an infinite 1D chain structure for 1.0 ML coverage and an infinite network extending over two dimensions for 1.5 ML. A third new structure, our 0.5 ML structure, is also a stable, low-energy structure. It was obtained by a simple (at least computationally) modification of the monolayer. All three are listed at the end of Table I and constitute the A, I and B cases in Table II.

B. Stability vs dissociation degree at 1.0 ML coverage

In the literature up to now, the 1.0 ML structures for $\text{H}_2\text{O}/\text{ceria}(111)$ have dealt with Q-0.0 and Q-1.0, plus the Q-0.25 structure of Kropp *et al.* Here, we explore Q-0.0, 0.25, 0.50, 0.75, and 1.0. Figure 3 displays the adsorption energy per water molecule with respect to the degree of dissociation, Q, for our various variants of the monolayer coverage. The lowest-energy structures are interpolated with a line to highlight the convex hull. The inset shows the adsorption energy with respect to coverage. In it, the 1.0 ML is more stable than the structures found at both lower and higher coverages. All the data in the figure are also given in Table II.

At 1.0 ML coverage, in the system of fully intact water molecules (Q-0), two stable structures were found (labeled 4 and 5 in Fig. 3). Although the adsorption energy difference is negligible (0.003 eV, i.e., the same in the convergence criterion) they show different bonding motifs. In structure 5 all water molecules bind to the surface but not to each other. Structure 4 is stabilized by forming H-bonded dimers but this will simultaneously destabilize the water-surface bonds. The net result is that 4 and 5 have virtually the same adsorption energy. Our attempts to extend the H-bond network were unsuccessful due to the large distances between adsorption sites. Upon geometry optimization of tested water chains, they reverted back to isolated water molecules or dimers.

This limitation is overcome by partial dissociation of the surface water species. The OH_f ions allow for an increased flexibility of H-bond geometries. A mix of intact and dissociated water molecules can then form H-bonded networks involving more than two water

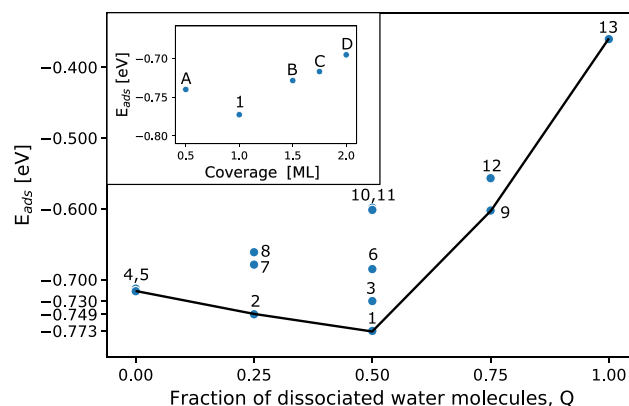


FIG. 3. Adsorption energy of water on the ceria(111) surface. The main figure shows 13 cases of 1.0 ML coverage where E_{ads} is plotted against the fraction of dissociated water molecules, Q. The solid line connects the lowest energy structures. The inset shows the adsorption energy with respect to coverage in ML, displaying the most stable structures for each coverage. Numbers and letters refer to those listed in Table II.

molecules, and we find H-bonded tetramers at Q-0.25 and the 1D-chain described above at Q-0.5. Dissociation at Q-0.5 yields the most stable structure. From previous studies, we believe that hydrogen bonds strengths are generally ordered as $\text{HOH}\cdots\text{OH}_f > \text{HOH}\cdots\text{OH}_2 > \text{OH}_f\cdots\text{OH}_2$ (see Fig. 5 in Ref. 41). At Q-0.5, the number of strong hydrogen bonds can be maximized, as in the case of our 1.0 ML chain structure.

With increasing dissociation, destabilization from increasing hydroxide interactions occur but is initially stabilized by favorable hydrogen bonds in the adsorbed layer. As the dissociation surpasses Q-0.5, the possibilities for hydrogen bonding diminish and the destabilization will dominate. Note, however, that the energy differences between many structures at 1.0 ML coverage are small, as exemplified in Fig. 3, which is attributed to different hydrogen-bond arrangements. In reality, many of these structures may come into play simultaneously, even at low temperatures.

C. Comparison with experimental TPD

At least four experimental TPD studies of water desorption from the stoichiometric $\text{CeO}_2(111)$ surface have been published in the literature, as mentioned in the Introduction. Supported by XPS investigations, several spectral features have been identified and discussed, namely, a broad water peak, roughly centered around 200 K, and shifting toward lower temperatures for higher initial water coverage,^{6–9} and a smaller peak with a maximum in the range of 270–290 K.^{6–8} The latter peak has been interpreted as water molecules resulting from a re-combination of OH_f and O_3H hydroxide ions in an activated process, making it less connected to the adsorption energy and it will not be further discussed here. The broad large peak centered around 200 K has been interpreted as consisting of several contributions, namely, (i) a large peak below 200 K (maximum in the range 150–200 K in different studies^{5–9}), originating from multilayer water molecules not in contact with the oxide surface, and (ii) a shoulder believed to originate from the first-layer water molecules and peaking at about 200 K^{6,7,9} and for very small coverages even at higher temperatures.⁶

We have estimated the maximum position of the temperature programmed desorption peaks (simply denoted desorption temperatures here) based on our calculated structures and adsorption energies. A thermal correction was applied by adding the zero point energy contributions to the adsorption energy from the gas-phase water molecule and surface-bound water (decreasing the magnitude of the adsorption energy). This contribution was estimated from harmonic vibrational normal mode calculations that we performed using the *phonopy* package.⁴² We obtained values 0.093 and 0.089 eV/ H_2O for structures 1 and 4, which are 1 ML structures with Q-0.5 and Q-0.0, respectively (cf. Table II; the values in the table are the uncorrected values). Rather than explicitly calculating the contribution for each monolayer structure, a representative value of 0.090 eV/ H_2O was applied to all those adsorption energies in the TPD analysis. The value 0.090 eV/ H_2O is consistent with Hofmann and Sauer's findings in Ref. 39 and, as said, decreases the magnitude of the adsorption energy.

The Redhead equation⁴³ was then used to relate the adsorption energy with the desorption temperature using an experimentally determined prefactor, ν , of $10^{14.6}$ Hz, as given by Ref. 10, and a heating rate, β , of 2 K/s.

First, we estimated a desorption temperature from our calculated E_{ads} values in Table II for structures at coverages 1.0 ML (structure 1) and 2.0 ML (structure E) with the added thermal correction, subtracting one from the other according to $2 \cdot E_{ads,2.0\text{ML}} - E_{ads,1.0\text{ML}}$. This approach, one could say, yields a crude estimate of the “multilayer” feature (i) in the experimental TPD spectrum. Our desorption temperature obtained this way is 177 K, i.e., in the range of experimental observations (150–200 K).

Second, the desorption temperature for the water molecules in monolayer structure 1 was addressed. Our E_{ads} value here does not refer only to desorption of intact water molecules as it is an average over the 50% intact water and 50% hydroxide species. Accepting this conceptual mismatch (whose effect may be modest), our 1.0 ML E_{ads} value with the added thermal correction gives a desorption temperature of 227 K, slightly higher than the peak value of the comparable broad experimental peak (200 K).

In summary, our estimated desorption temperature values based on optPBE-vdW adsorption energies agree quite well with the experimental findings. Nevertheless, it should be noted that it is not straightforward to relate experimental desorption temperatures to adsorption energies (see, for example, the discussion by Campbell *et al.*¹⁰). Furthermore, the Redhead equation depends on the assumed parameter settings and will yield a 15 K shift in desorption temperature for an order of magnitude difference in the assumed parameters ν or β .

D. Surface energy

In order to compare the stabilities of surfaces with different water coverages, we have constructed a surface phase diagram (Fig. 4). The key quantity in the construction of such a diagram is the surface free energy, γ , as a function of the chemical potential of

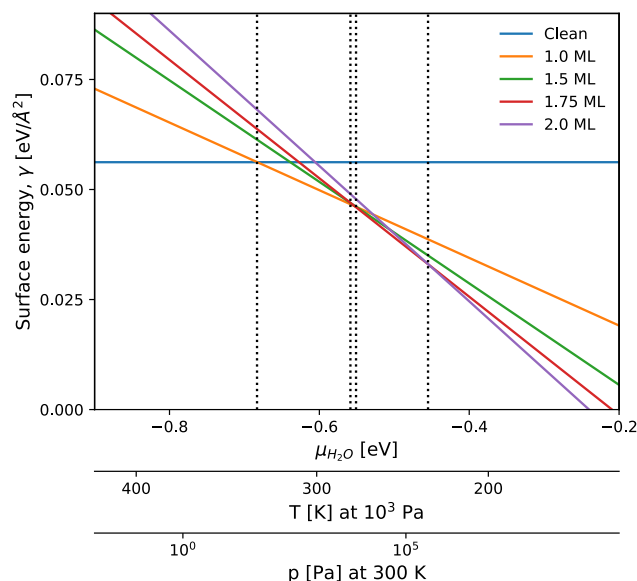


FIG. 4. Surface energy of the clean surface and at water coverages 1.0, 1.5, 1.75, and 2.0 ML as a function of water chemical potential. Vertical dotted lines mark the boundaries of the different stability regions (see text for further details).

water, $\mu[\text{H}_2\text{O}(\text{g})]$, which was calculated according to the following formula:

$$\gamma = (G[\text{H}_2\text{O}/\text{CeO}_2] - m \cdot G[\text{CeO}_2]_{\text{bulk}} - n \cdot \mu[\text{H}_2\text{O}(\text{g})]) / A - \gamma_{\text{opposite}}, \quad (2)$$

$$\gamma_{\text{opposite}} = (G[\text{CeO}_2] - m \cdot G[\text{CeO}_2]_{\text{bulk}}) / 2A, \quad (3)$$

where n is the number of water molecules in the system, A is the area, and m is the number of CeO_2 formula units in the slab supercell. $G[\text{H}_2\text{O}/\text{CeO}_2]$ and $G[\text{CeO}_2]$ are the free energy of the surface cell with and without water adsorbed on the ceria slab. $G[\text{CeO}_2]_{\text{bulk}}$ is the bulk free energy contribution per CeO_2 formula unit. Following standard procedures, we approximate the Gibbs free energy with the electronic (DFT) energy, and for $G[\text{H}_2\text{O}/\text{CeO}_2]$, the zero-point vibrational contributions of the adsorbate, described in Sec. III C, are added. We also assume that volume changes in the slab can be neglected. The chemical potential of gas-phase water is referenced to the electronic (DFT) energy and includes the rotational, translational, and vibrational contributions for an ideal gas and is a function of the temperature and pressure of the gas. In this work, we have calculated this dependence from thermodynamic tables⁴⁴ in accordance with Refs. 39 and 45. As water is adsorbed on one of the two exposed surfaces of the CeO_2 slab, the γ_{opposite} term needs to be included; it is the surface free energy contribution of the clean surface opposite to the surface of adsorbed water.

Figure 4 shows the resulting surface energy γ as a function of $\mu_{\text{H}_2\text{O}}$. It is seen that, at low chemical potentials of water, up to -0.68 eV, the clean surface is more stable than the water covered surfaces. At chemical potentials in the window from -0.68 to -0.55 eV, the 1.0 ML coverage dominates. For a higher chemical potential, the 1.5 ML coverage is stabilized in a narrow window around -0.55 eV after which 1.75 ML dominates. Above -0.46 eV, the 2.0 ML coverage is stabilized.

In conclusion, our calculations suggest the monolayer could dominate under ambient conditions of 300 K and 10^3 Pa, where the latter value was selected to represent a typical water pressure at ambient conditions. At room temperature and ultrahigh vacuum, a clean surface would be expected. It is further noted that lowering the temperature or increasing the pressure results in a gradual buildup of thicker layers.

IV. CONCLUSION

In previous quantum-mechanical studies of thin film water adsorption on ceria(111), up to and including 1.0 ML coverage, much emphasis has been placed on the largely spaced ceria sublattice that tends to hinder efficient hydrogen bonding between the water molecules, making them essentially isolated, regardless of whether they are dissociated or not. One exception is the finite surface clusters observed in the QM calculations of Ref. 21. In the present study, we have investigated thirteen 1.0 monolayer structures with the aim to search for extended hydrogen-bonded networks and explore the influence of water dissociation on the interface stability. We report a new structure for the 1.0 ML coverage, consisting of a one-dimensional $\cdots\text{OH}_f\cdots\text{HOH}\cdots\text{OH}_f\cdots\text{HOH}\cdots$ chain with an infinite hydrogen-bonded network in one dimension. This is the most stable structure reported for 1.0 ML on ceria(111). At 1.5 ML, we found

another hydrogen-bond network, this time spanning the two surface dimensions.

We also related the adsorption energies for the first layer and for multilayer adsorption to experimental TPD measurements, finding a close agreement between our zero-point energy corrected E_{ads} values calculated at the optPBE-vdW level, and experimental results. Finally, we calculated the stability windows for our 1.0 and 1.5 ML structures plus for two higher-coverage structures at 1.75 and 2.0 ML, taken from the literature. With our computational method, the structure at 1.0 ML is the stable phase under ambient conditions ($T = 300$ K, $p_{\text{H}_2\text{O}} = 10^3$ Pa).

ACKNOWLEDGMENTS

We would like to acknowledge the support from the Swedish Research Council (Vetenskapsrådet) and the National Strategic e-Science program eSENCE. The simulations were performed on resources provided by the Swedish National Infrastructure for Computing (SNIC) at HPC2N and NSC.

REFERENCES

- 1 R. Mu, Z. J. Zhao, Z. Dohnálek, and J. Gong, "Structural motifs of water on metal oxide surfaces," *Chem. Soc. Rev.* **46**, 1758–1806 (2017).
- 2 D. R. Mullins, "The surface chemistry of cerium oxide," *Surf. Sci. Rep.* **70**, 42–85 (2015).
- 3 T. Wu, Q. Deng, H. A. Hansen, and T. Vegge, "Mechanism of water splitting on gadolinium-doped $\text{CeO}_2(111)$: A DFT + U study," *J. Phys. Chem. C* **123**, 5507–5517 (2019).
- 4 M. Fronzi, M. H. N. Assadi, and D. A. Hanaor, "Theoretical insights into the hydrophobicity of low index CeO_2 surfaces," *Appl. Surf. Sci.* **478**, 68–74 (2019).
- 5 F. Caputo, M. Mameli, A. Sienkiewicz, S. Licocchia, F. Stellacci, L. Ghibelli, and E. Traversa, "A novel synthetic approach of cerium oxide nanoparticles with improved biomedical activity," *Sci. Rep.* **7**, 4636 (2017).
- 6 M. A. Henderson, C. L. Perkins, M. H. Engelhard, S. Thevuthasan, and C. H. Peden, "Redox properties of water on the oxidized and reduced surfaces of $\text{CeO}_2(111)$," *Surf. Sci.* **526**, 1–18 (2003).
- 7 D. R. Mullins, P. M. Albrecht, T. L. Chen, F. C. Calaza, M. D. Biegalski, H. M. Christen, and S. H. Overbury, "Water dissociation on $\text{CeO}_2(100)$ and $\text{CeO}_2(111)$ thin films," *J. Phys. Chem. C* **116**, 19419–19428 (2012).
- 8 V. Matolín, I. Matolínová, F. Dvořák, V. Johánek, J. Mysliveček, K. C. Prince, T. Skála, O. Stetsovych, N. Tsud, M. Václavů, and B. Šmíd, "Water interaction with $\text{CeO}_2(111)/\text{Cu}(111)$ model catalyst surface," *Catal. Today* **181**, 124–132 (2012).
- 9 B. Chen, Y. Ma, L. Ding, L. Xu, Z. Wu, Q. Yuan, and W. Huang, "Reactivity of hydroxyls and water on a $\text{CeO}_2(111)$ thin film surface: The role of oxygen vacancy," *J. Phys. Chem. C* **117**, 5800–5810 (2013).
- 10 C. T. Campbell and J. R. V. Sellers, "Enthalpies and entropies of adsorption on well-defined oxide surfaces: Experimental measurements," *Chem. Rev.* **113**, 4106–4135 (2013).
- 11 S. Gritschneider and M. Reichling, "Structural elements of $\text{CeO}_2(111)$ surfaces," *Nanotechnology* **18**, 044024 (2007).
- 12 S. Torbrügge, O. Custance, S. Morita, and M. Reichling, "Manipulation of individual water molecules on $\text{CeO}_2(111)$," *J. Phys.: Condens. Matter* **24**, 084010 (2012).
- 13 J. Paier, C. Penschke, and J. Sauer, "Oxygen defects and surface chemistry of ceria: Quantum chemical studies compared to experiment," *Chem. Rev.* **113**, 3949–3985 (2013).
- 14 H. T. Chen, Y. M. Choi, M. Liu, and M. C. Lin, "A theoretical study of surface reduction mechanisms of $\text{CeO}_2(111)$ and (110) by H_2 ," *ChemPhysChem* **8**, 849–855 (2007).

- ¹⁵M. B. Watkins, A. S. Foster, and A. L. Shluger, "Hydrogen cycle on CeO₂(111) surfaces: Density functional theory calculations," *J. Phys. Chem. C* **111**, 15337–15341 (2007).
- ¹⁶S. Kumar and P. K. Schelling, "Density functional theory study of water adsorption at reduced and stoichiometric ceria (111) surfaces," *J. Chem. Phys.* **125**, 204704 (2006).
- ¹⁷M. Fronzi, S. Piccinin, B. Delley, E. Traversa, and C. Stampfl, "Water adsorption on the stoichiometric and reduced CeO₂(111) surface: A first-principles investigation," *Phys. Chem. Chem. Phys.* **11**, 9188–9199 (2009).
- ¹⁸M. Molinari, S. C. Parker, D. C. Sayle, and M. S. Islam, "Water adsorption and its effect on the stability of low index stoichiometric and reduced surfaces of ceria," *J. Phys. Chem. C* **116**, 7073–7082 (2012).
- ¹⁹D. Fernández-Torre, K. Kośmider, J. Carrasco, M. V. Ganduglia-Pirovano, and R. Pérez, "Insight into the adsorption of water on the clean CeO₂(111) surface with van der Waals and hybrid density functionals," *J. Phys. Chem. C* **116**, 13584–13593 (2012).
- ²⁰Z. Yang, Q. Wang, S. Wei, D. Ma, and Q. Sun, "The effect of environment on the reaction of water on the ceria(111) surface: A DFT+U study," *J. Phys. Chem. C* **114**, 14891–14899 (2010).
- ²¹T. Kropp, J. Paier, and J. Sauer, "Interactions of water with the (111) and (100) surfaces of ceria," *J. Phys. Chem. C* **121**, 21571–21578 (2017).
- ²²G. Carchini, M. García-Melchor, Z. Łodziana, and N. López, "Understanding and tuning the intrinsic hydrophobicity of rare-earth oxides: A DFT+U study," *ACS Appl. Mater. Interfaces* **8**, 152–160 (2016).
- ²³M. Farnesi Camellone, F. Negreiros Ribeiro, L. Szabová, Y. Tateyama, and S. Fabris, "Catalytic proton dynamics at the water/solid interface of ceria-supported Pt clusters," *J. Am. Chem. Soc.* **138**, 11560–11567 (2016).
- ²⁴D. Marrocchelli and B. Yildiz, "First-principles assessment of H₂S and H₂O reaction mechanisms and the subsequent hydrogen absorption on the CeO₂(111) surface," *J. Phys. Chem. C* **3**, 2411–2424 (2012).
- ²⁵L. Szabová, Y. Tateyama, V. Matolin, and S. Fabris, "Water adsorption and dissociation at metal-supported ceria thin films: Thickness and interface-proximity effects studied with DFT+U calculations," *K. Phys. Chem. C* **5**, 2537–2544 (2015).
- ²⁶C. W. Castleton, J. Kullgren, and K. Hermansson, "Tuning LDA+U for electron localization and structure at oxygen vacancies in ceria," *J. Chem. Phys.* **127**, 244704 (2007).
- ²⁷G. Kresse and J. Hafner, "Ab initio molecular dynamics for liquid metals," *Phys. Rev. B* **47**, 558–561 (1993).
- ²⁸G. Kresse and J. Hafner, "Ab initio molecular-dynamics simulation of the liquid-metalamorphous- semiconductor transition in germanium," *Phys. Rev. B* **49**, 14251–14269 (1994).
- ²⁹G. Kresse and J. Furthmüller, "Efficiency of *ab-initio* total energy calculations for metals and semiconductors using a plane-wave basis set," *Comput. Mater. Sci.* **6**, 15–50 (1996).
- ³⁰G. Kresse and J. Furthmüller, "Efficient iterative schemes for *ab initio* total-energy calculations using a plane-wave basis set," *Phys. Rev. B* **54**, 11169–11186 (1996).
- ³¹J. Klimeš, D. R. Bowler, and A. Michaelides, "Chemical accuracy for the van der Waals density functional," *J. Phys.: Condens. Matter* **22**, 022201 (2010).
- ³²J. Klimeš, D. R. Bowler, and A. Michaelides, "Van der Waals density functionals applied to solids," *Phys. Rev. B* **83**, 195131 (2011).
- ³³G. G. Kebede, D. Spångberg, P. D. Mitev, P. Broqvist, and K. Hermansson, "Comparing van der Waals DFT methods for water on NaCl(001) and MgO(001)," *J. Chem. Phys.* **146**, 064703 (2017).
- ³⁴G. Kebede, P. D. Mitev, P. Broqvist, A. Eriksson, and K. Hermansson, "Fifty shades of water: Benchmarking DFT functionals against experimental data for ionic crystalline hydrates," *J. Chem. Theory Comput.* **15**, 584–594 (2019).
- ³⁵P. E. Blöchl, "Projector augmented-wave method," *Phys. Rev. B* **50**, 17953–17979 (1994).
- ³⁶G. Kresse and D. Joubert, "From ultrasoft pseudopotentials to the projector augmented-wave method," *Phys. Rev. B* **59**, 1758–1775 (1999).
- ³⁷S. Dudarev and G. Botton, "Electron-energy-loss spectra and the structural stability of nickel oxide: An LSDA+U study," *Phys. Rev. B* **57**, 1505–1509 (1998).
- ³⁸J. Tersoff and D. R. Hamann, "Theory of the scanning tunneling microscope," *Phys. Status Solidi A* **31**, 805–813 (1985).
- ³⁹A. Hofmann and J. Sauer, "Surface structure of hydroxylated and sulfated zirconia. A periodic density-functional study," *J. Phys. Chem. B* **108**, 14652–14662 (2004).
- ⁴⁰R. Mu, D. C. Cantu, V. A. Glezakou, I. Lyubnitsky, R. Rousseau, and Z. Dohnálek, "Deprotonated water dimers: The building blocks of segmented water chains on rutile RuO₂(110)," *J. Phys. Chem. C* **119**, 23552–23558 (2015).
- ⁴¹K. Hermansson, P. A. Bopp, D. Spångberg, L. Pejov, I. Bakó, and P. D. Mitev, "The vibrating hydroxide ion in water," *Chem. Phys. Lett.* **514**, 1–15 (2011).
- ⁴²A. Togo and I. Tanaka, "First principles phonon calculations in materials science," *Scr. Mater.* **108**, 1–5 (2015).
- ⁴³P. A. Redhead, "Thermal desorption of gases," *Vacuum* **12**, 203–211 (1962).
- ⁴⁴M. W. Chase, C. A. Davies, J. R. Downey, D. J. Frurip, R. A. McDonald, and A. N. Syverud, "NIST-JANAF thermochemical tables," *J. Phys. Chem. Ref. Data Monogr.* **9**, 1 (1998).
- ⁴⁵K. Reuter and M. Scheffler, "Composition, structure, and stability of RuO₂(110) as a function of oxygen pressure," *Phys. Rev. B* **65**, 035406 (2001).